



# Tsunamigenic potential of unstable masses in the Gulf of Pozzuoli, Campi Flegrei, Italy

Filippo Zaniboni<sup>1</sup>, Luigi Sabino<sup>2</sup>, Cesare Angeli<sup>1</sup>, Martina Zanetti<sup>1</sup> and Alberto Armigliato<sup>1</sup>

<sup>1</sup> Department of Physics and Astronomy “A. Righi”, Alma Mater Studiorum - University of Bologna, Bologna, 40127, Italy

<sup>2</sup> Department of Mathematics and Physics, University of Campania “L. Vanvitelli”, Caserta, 81100, Italy

Correspondence to: Filippo Zaniboni (filippo.zaniboni@unibo.it)

**Abstract.** Campi Flegrei, one of the most monitored and studied volcanic areas in the world, has recently attracted significant attention due to the reactivation of its peculiar activity, consisting into small earthquakes, geothermal phenomena and slow subsidence/rapid uplift cycles, known as bradyseism. While much of the research and of the attention focuses on volcanic manifestations, the potential hazard posed by gravitational instabilities has received little consideration. The interaction of the destabilized masses with water can trigger tsunamis, potentially affecting the whole coastline of the Gulf of Pozzuoli, which lies above the Campi Flegrei caldera. Moving from the limited available geomorphological studies of the area, a set of four scenarios (three submarine and one subaerial) are here reconstructed. These are simulated through a sequence of numerical codes, accounting for all the phases of the tsunami process, providing insights into the distribution of tsunami energy and identifying the most affected coastal stretches. Additionally, the study explores the influence of dispersion effects in the tsunami propagation and the occurrence of resonance effects in some minor inlets of the Gulf, emphasizing the importance of accounting for complex and non-linear coastal processes when treating with landslide-generated tsunamis.

## 1 Introduction

The recent strengthening of the Campi Flegrei activity has raised many concerns about the potential impacts of volcanic-related manifestations on local population and infrastructures. The caldera, located in correspondence of an extremely densely inhabited area in the surroundings of Naples (South Italy), is one of the most active and dangerous in the world. The study of the hazard correlated to the Campi Flegrei activity, concerning the tephra dispersal in case of eruption, has been already treated in the scientific literature (Selva et al., 2018). On this basis, a National Civil Protection plan has been realized in case of emergency (<https://mappe.protezionecivile.gov.it/en/risks-maps-and-dashboards/national-planning-phlegraean-fields/>). Other considered potential hazards linked to the eruption of the Campi Flegrei caldera are pyroclastic flows (Neri et al., 2015), phreatic explosions (Mayer et al., 2016) and mud flows generated by the interaction between the ash ejected from the volcano and the rain (Isaia et al., 2021). Earthquakes are frequent, though characterized by low magnitude. As an example, according to the December 2024 INGV - Osservatorio Vesuviano bulletin (<https://www.ov.ingv.it/index.php/flegrei-stato-attuale>), 273



30 events have been recorded during the month. Over 93% of these had magnitude lower than 1, four exceeded  $M_d = 2.0$  and  
31 the maximum was 3.4.

32 The interaction of volcanic activity with the sea and the consequent generation of tsunamis received some attention as well:  
33 the work by Paris et al. (2019) tested the effects of submarine volcanic explosions in the Gulf of Pozzuoli by means of  
34 numerical scenarios and a Probabilistic Tsunami Hazard Analysis (PTHA) methodology. Grezio et al. (2020) attempted a  
35 comprehensive approach including earthquakes, submarine landslides and volcanic explosions as potential sources for tsunami  
36 generation affecting the Gulf of Naples, implementing them into a PTHA providing hazard curves for different localities along  
37 the coasts.

38 In the specific, gravitational collapses are one of the least considered potential sources of natural hazards in the area. Volcanic  
39 activity at Campi Flegrei can induce instability both in the short term, through seismic shaking, and in the long term, due to  
40 slope steepening associated with the caldera uplift. The scenarios considered in Grezio et al. (2020) were purely synthetic,  
41 without evaluation of geological and morphological evidence, of the sliding dynamics and of possible hydrodynamic effects  
42 during the tsunami propagation.

43 This work aims to bridge to fill these gaps, assessing the tsunamigenic potential of local submarine and subaerial landslides,  
44 evaluating the tsunami distribution patterns and the respective impact on the coasts, at the scale of the Gulf of Pozzuoli basin.  
45 The masses generating the waves are selected based on a worst-case credible approach (see e.g. Zaniboni and Armigliato,  
46 2025), which relies on the present morphology and on the existing knowledge of the mass transport processes in the area. The  
47 tsunami hazard is then assessed through a set of numerical codes, already tested and applied in many other landslide-tsunami  
48 cases. This investigation has been preliminarily performed and reported in Sabino (2024): here it is extended including the role  
49 of dispersion in the tsunami propagation, since it can have significant influence in the impact of the waves on the coasts.

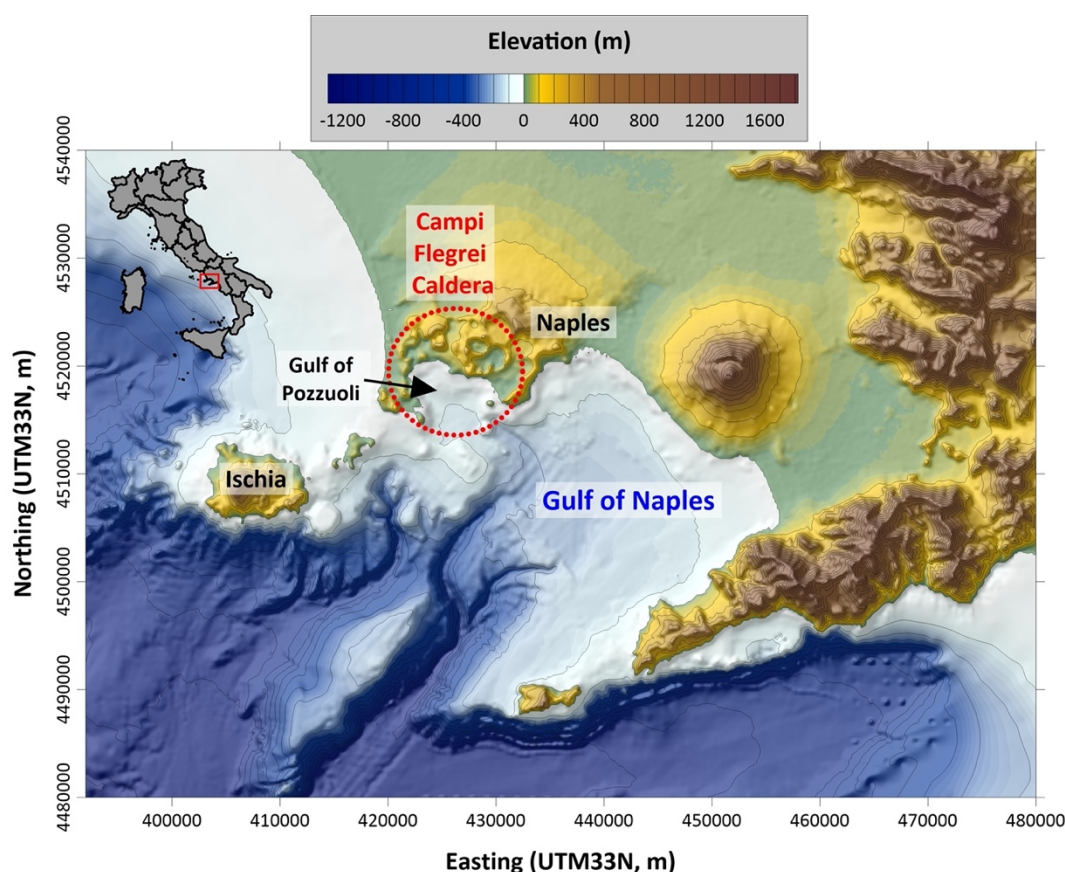
## 50 1.1 Campi Flegrei volcano

51 Campi Flegrei is a complex volcanic system with a history spanning at least the last 78,000 years (Perrotta et al., 2006),  
52 characterized by intense unrest episodes involving ground deformation and seismicity (de Natale et al., 2006), together with  
53 explosive eruptions and variable vent locations (Bevilacqua et al., 2015). Seismic studies have revealed a large magmatic sill  
54 at depth, potentially connected to the surface through deep fractures (Zollo et al., 2008). The heart of Campi Flegrei is the vast  
55 caldera, an almost circular structure with a diameter of about 10 km (marked by the red dashed line in Figure 1) involving the  
56 western districts of Naples in its subaerial expression, with a total potentially affected population of more than 360 thousand,  
57 living in the cities of Pozzuoli, Bagnoli and Bacoli. The submarine part of the caldera is covered by the Gulf of Pozzuoli, a  
58 small, shallow water sub-basin of the wider Gulf of Naples. The landscape of this area has been shaped by several volcanic  
59 events: the caldera was formed by a catastrophic volcanic explosion that occurred approximately 39,000 years ago. This event,  
60 an eruption of 100-200 km<sup>3</sup> of rock called "Ignimbrite Campana" (Rosi et al., 1983; Perrotta et al. 2006), shaped the region's  
61 topography, creating a unique landscape characterized by hills, fumaroles, and hot springs. At the centre of the caldera rises  
62 the Solfatara crater, a focal point for the volcanic and geothermal activity in the area. Historical reports from Roman times



63 reveal a general trend of slow subsidence (rate of about 1-2 cm/yr), alternated with occasional episodes of faster uplift (Di Vito  
64 et al., 2016; De Vivo et al., 2020), a peculiar behaviour that took the name of “bradyseism”. Soil subsidence can lead to coastal  
65 flooding, as testified by the submerged park of Baia, where Roman houses and constructions are still visible now at 6-8 m  
66 depth. The last significant eruption of Campi Flegrei caldera occurred in 1538, with 0.03 km<sup>3</sup> of erupted products that gave  
67 rise to the hill of Monte Nuovo in one single night (De Vivo et al., 2001). After that, the floor of the caldera underwent slow  
68 and regular subsidence. In more recent times, some episodes of uplift interrupted this phase: 74 cm in 1950-52, 159 cm in  
69 1970-72 and 178 cm in 1982-84 (Del Gaudio et al., 2010), resulting in a maximum rise of about 3.5 meters of the ground in  
70 the city of Pozzuoli, with shallow micro-seismicity recorded in response to fluid movement episodes.

71



72

73

74 **Figure 1. Morphological map of the Gulf of Naples (South Italy). The red-dashed circle delimits approximately the Campi Flegrei**  
75 **caldera, involving a subaerial part (west of Naples) and a submarine portion (Gulf of Pozzuoli).**

76 Starting from the second half of 2023, the bradyseism has resumed, with seismic activity intensifying, although most of the  
77 events were characterized by low magnitudes (about 90% of the events had magnitudes less than 1.0, see



78 <https://www.ov.ingv.it/index.php/monitoraggio-e-infrastrutture/bollettini-tutti/bollett-mensili-cf>), with maximum depths of  
79 around 4 km, predominantly concentrated within the first 2 km (Danesi et al., 2024). The sequence culminated with the seismic  
80 events on September 27<sup>th</sup>, 2023 ( $M_d = 4.2$ ) and October 2<sup>nd</sup>, 2023 ( $M_d = 4.0$ ), located respectively in the area between Bagnoli  
81 and Pozzuoli and in the Pisciarelli-Solfatara area.

## 82 **2 Data and methods**

83 The investigation on the tsunami hazard in the gulf of Pozzuoli associated to the Campi Flegrei activity, triggering potential  
84 instabilities interacting with water, is here performed through numerical methods, which in turn implement approaches that  
85 are described in this section. An initial necessary premise concerns the importance of considering the dispersive effects in  
86 landslide-tsunami simulations, a task that is usually underestimated but whose effects could be relevant in the analysis of the  
87 tsunami impact on the coast.

### 88 **2.1 Landslide-tsunamis and dispersive effects**

89 Tsunamis are oscillations induced by a perturbation of the equilibrium state involving the whole water body, which can be  
90 produced by sudden changes in the sea bottom (earthquakes, submarine landslides, underwater volcanic explosions) or upon  
91 the sea surface (subaerial landslides, atmospheric perturbations, cosmogenic tsunamis).

92 In general, in hydrodynamics, each wave is subject to the dispersion relation, linking the phase velocity  $c$  to the wave number  
93  $k$  (or to its inverse, the wavelength  $\lambda$ ): the smaller is the second (i.e., the bigger is the wavelength), the higher is the first. In  
94 short, longer oscillations are faster than shorter ones (for a general overview about this topic see for example Saito, 2019).

95 A tsunami can be considered mostly as a “packet” of waves, meaning that it is not a monochromatic wave, but it results from  
96 the superposition of different components, each characterized by a specific wavelength, then with its own velocity. When  $\lambda$  is  
97 much bigger than the water depth  $h$  of the involved basin, the hydrodynamic equations can be significantly simplified by  
98 means of the shallow-water (SW) approach, in which tsunamis are treated as “long-waves”. This is generally valid for waves  
99 generated by earthquakes, since the source has dimensions that is usually much bigger than the typical depth of the sea. When  
100 the tsunami trigger is provided by other phenomena, such as landslides, SW is known to neglect important hydrodynamic  
101 effects, such as dispersion, that can affect significantly the wave propagation and impact on the coast. It is generally agreed  
102 that SW is considered proper when the ratio  $\lambda/h$  is bigger than 20, while for lower values (i.e. for “shorter” waves) a more  
103 sophisticated and higher-order version of the hydrodynamic equations should be considered, as for example the Boussinesq  
104 approximation (hereafter accounted for as non-hydrostatic approach, NH).

105 A quantification of the dispersive effects on the tsunami propagation was attempted in Glimsdal et al. (2013). A rearrangement  
106 of the considerations found in that work leads to the estimation of the ratio between distance and initial signal wavelength for  
107 which the dispersion becomes relevant and cannot be neglected anymore. Calling this (non-dimensional) dispersion distance  
108 as  $D$ , the expression is:



$$D = 0.025 \cdot \left(\frac{\lambda}{h}\right)^2 \quad (1)$$

For “long waves”, then,  $\lambda/h \approx 20$  and  $D \approx 10$ : dispersive effects manifest at least at a distance ten times the initial wavelength. Table 1 reports some typical values for wavelengths and water basin depths found respectively for: earthquake-tsunamis (first line), for which generally SW approach is applicable; submarine landslide tsunamis (second line) for which SW is valid only on limited domains; subaerial landslide tsunamis (third line), which can be considered in general as deep-water (DW) waves, for which the NH approach is more suitable.

In general, we can see that dispersion affects every tsunami, also the “longer” ones, but it manifests only on very long distances, where probably the perturbation itself has already been damped by other propagation effects. Neglecting dispersion means that the different components of the tsunami travel all together and impact the coast at the same time; conversely, when considering it, the longer components travel much faster than the shorter ones. This provokes an “unpacking” of the tsunami, that is much more evident and effective with increasing distance from the source: in general, then, neglecting dispersion causes an overestimation of the tsunami effects.

**Table 1. Examples of waves and of computing of respective dispersion distance.  $\lambda$ : initial wavelength;  $h$ : water depth;  $D$ : dispersion distance, computed by Eq. (1);  $d$ : distance for which dispersion effects become predominant ( $d = D \cdot \lambda$ ).**

$\lambda$ (km)	$h$ (m)	$\lambda/h$	Wave type	$D$	$d$ (km)
100	4000	25	SW	15.6	1562.5
5	500	10	Weakly SW	2.5	12.5
1	200	5	DW	0.625	0.625

## 2.2 Overview on numerical techniques

Landslide-generated tsunamis are highly complex processes. Assessing their impact on the coast through numerical simulations requires numerous approximations and assumptions. The approach adopted here divides the entire process into distinct phases: i) the landslide motion, ii) the transfer of energy from the mass to the water, iii) tsunami propagation, and iv) the wave's impact on the coast. Each phase is treated independently, with no back-interactions considered (for example, the mass-water interaction, where the wave's propagation can alter the water column and influence the dynamics of the landslide on the seafloor, is neglected in this study). The phases are addressed sequentially, with the output of one stage serving as the input for the next.

*Landslide motion.* The movement of the mass along the seafloor triggers the tsunami. Unlike earthquake-generated tsunamis, where the source process can be considered instantaneous relative to the wave's propagation (at least as a first approximation), landslide-tsunamis involve a finite time for the generation phase. Thus, it is essential to accurately describe the mass dynamics and the evolution of shape changes. This is achieved using the numerical code UBO-BLOCK (see detailed description in Tinti





et al., 1997), which divides the sliding mass into interacting portions. The equation governing the centre of mass (CoM) motion is determined by the forces acting on the mass: gravity, buoyancy, basal friction, surface drag, and an internal interaction force accounting for energy dissipation due to deformation. The resulting time-series of geometric and dynamic quantities describing the landslide motion is then generated. Applications of UBO-BLOCK to landslide-tsunami events can be retrieved in Tryantafillou et al. (2020), Zaniboni et al. (2021), Gallotti et al. (2021), Gasperini et al. (2022), Gallotti et al. (2023), Zaniboni et al. (2024) and in the references therein.

*Tsunamigenic impulse.* The next step involves assessing the perturbation to the water column caused by the sliding motion along the seafloor. This disturbance provides the dynamic forcing term for the wave propagation equations, which are not instantaneous but evolve over time. The change in the seafloor due to the landslide is interpolated onto the tsunami grid nodes, with a filter applied to local sea depths that suppresses high frequencies. These tasks are handled by the intermediate code UBO-TSUIMP (details in Tinti et al., 2006).

*Tsunami propagation and coastal impact.* The final two phases are simulated using the JAGURS code, which solves the fluid dynamics equations using finite difference methods. Tsunami propagation can be modelled using either the shallow-water (SW) equations or a more sophisticated approach that accounts for vertical variations in hydrodynamic quantities, implementing for example the Boussinesq model (NH). The non-hydrostatic method allows the code to capture dispersion effects, which are crucial for landslide-generated tsunamis, as described in Section 1.1. JAGURS supports simulations over computational grids with varying resolutions (using a nested grid approach) and can model coastal inundation. It is also optimized for parallel computing with MPI and OpenMPI coding, enabling the simulation of dispersive effects over large computational domains (see Baba et al., 2015, for further description). While JAGURS is widely used for earthquake-generated tsunamis (Ren et al., 2021; Ehara et al., 2023), for landslide-generated events it requires some adaptations, due to the nature of the phenomenon itself. As previously mentioned, the tsunamigenic impulse for landslide-tsunamis is not instantaneous: then, it must be provided to the code as a sequence of single impulses, one for each time step describing the landslide motion along the sea bottom and producing the perturbation.

## 2.3 Computational grid

The numerical codes applied here require as input a regularly spaced computational grid, whose definition and assembling needs a compromise among different aspects: the detailed description of the morphology, mainly for the coastal areas, requires a huge number of nodes, that on the contrary needs to be limited basing on the computational resources available. Additionally, landslide-tsunamis are known to affect limited domains, due to the dispersive effects characterizing their oscillations that produce a rapid damping of their amplitude. In the specific case studied here, the morphology of the seabed suggests that the mass instabilities induced by the Campi Flegrei activity have typically small volumes, producing waves that will presumably travel modest distances, with reduced consequences on the coasts. Under all these considerations, the selected tsunami computational domain covers the Pozzuoli Gulf for an area of 12 km x 11 km approximately, with a spatial step of 20 m and



168 a total number of nodes of about 340 thousand (see Table 2). Raw data have been retrieved from the database MaGIC for the  
169 coastline and the bathymetry (DPC), and from the database Tinitaly (Tarquini et al., 2023) as concerns the topography.  
170 The morphology represented in Figure 2 shows some remarkable features as concerns landslide-tsunami triggering and  
171 propagation: i) the underwater slopes are in general quite gentle, inhibiting high initial acceleration of the sliding masses, one  
172 of the most important factors in tsunami genesis (e.g. Lovholt et al., 2015). Only the areas close to the Gulf’s mouth opposite  
173 sides, i.e. Capo Miseno on the west and Nisida Bank on the east (see Figure 2 for toponyms), show steep submarine gradients.  
174 ii) the coastal slope is generally flat, favoring water ingression and tsunami penetration; only the two abovementioned areas  
175 (Capo Miseno and Nisida) are characterized by steep coastal profiles, that can also produce rapidly moving collapses into the  
176 water. iii) the sea is rather shallow within the Gulf, with maximum depth reaching about 100 m, while it deepens eastward and  
177 southward. This will have consequences on the wave propagation in the basin, since, as we have seen, the sea depth deeply  
178 influences the tsunami behaviour during the propagation. iv) finally, but not less importantly, at this level of detail it is possible  
179 to represent the main piers and harbour structures (well visible at Pozzuoli and Bagnoli, Figure 2), which influence the wave  
180 propagation with local effects, such as for example multiple reflections and resonance.

181

182 **Table 2. Parameters of the tsunami computational domain covering the Gulf of Pozzuoli:**  
183  **$N_x$ , number of nodes in the west-east direction;  $N_y$ , number of nodes in the north-south direction;  $\Delta x, \Delta y$  spatial grid step along the**  
184  **$x$  and  $y$  directions respectively;  $N_{TOT}$ , total number of nodes;  $h_{max}$  maximum water depth in the computational grid.**

185

186

187

188

$N_x$	$N_y$	$\Delta x, \Delta y$ (m)	$N_{TOT}$	$h_{max}$ (m)
601	576	20	346 176	169

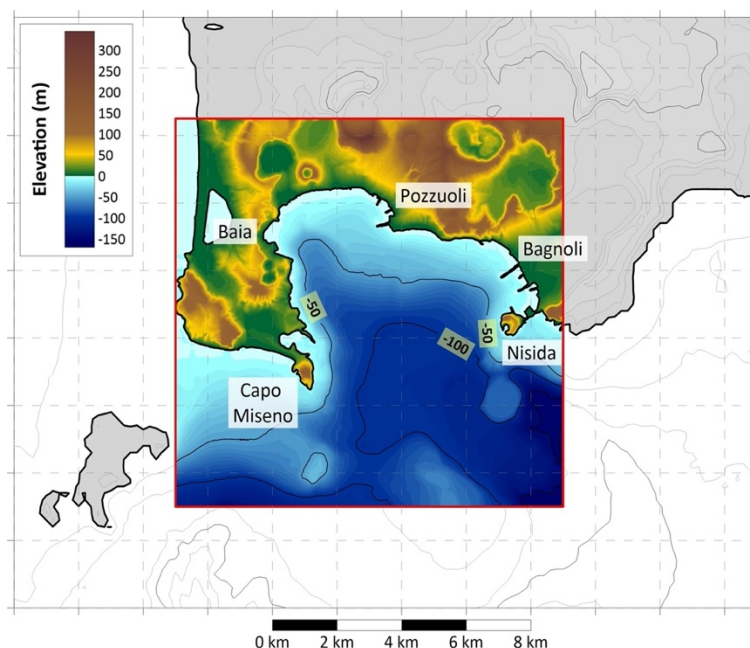


**Figure 2. Computational grid for the tsunami simulation, covering the Gulf of Pozzuoli with a spatial step of 20 m.**

### 3. Results

The evaluation of the landslide-tsunami hazard in the Gulf of Pozzuoli requires, as a first step, to identify the sources, i.e. masses that have the potential to generate waves, both in the submarine and in the subaerial environments. This investigation is here performed through a scenario approach, meaning that the sources are hypothesized starting from geological and morphological evidence, studying their signatures (scars, slopes, deposits) and the ensuing tsunamis evaluated through the numerical routine previously illustrated. The assumption is that such scenarios represent the range of possible and credible worst events occurring in the area, following the approach called Worst-case Credible Tsunami Hazard Assessment (WCTHA, Zaniboni and Armigliato, 2025), which is suitable to phenomena like landslide-tsunamis, where neither recurrence time are defined nor extensive catalogues of events are available, contrary to the most adopted approach in tsunami science (PTHA, see e.g. Behrens et al., 2021).

In the following, as a first step, the search for mass collapse traces in the Gulf of Pozzuoli within the scientific literature is reported; from this, a set of numerical scenarios is defined and the numerical routine previously described applied, providing a quantification of the hazard associated to the generated tsunamis.

#### 3.1 Mass instabilities in the Gulf of Pozzuoli and landslide scenarios

Recent magnetic surveys in the Gulf of Naples evidenced the presence of consistent deposits on the seabed, testifying an intense mass transport activity in the whole area (de Ritis et al., 2024), that could have probably generated tsunamis affecting





also the Gulf of Pozzuoli. The focus, though, is here centred on local sources, i.e. potential landslides triggered by the seismic shaking related to the Campi Flegrei caldera, then along the slopes (submarine and subaerial) in the Gulf of Pozzuoli area. As already mentioned, this is a small, shallow water basin, whose detailed stratigraphic and morphological features have been revealed by high-resolution seismic and bathymetric surveys (Aiello et al., 2012; Aiello et al., 2016; Somma et al., 2016). The area is characterized by numerous seismic units, both volcanic and sedimentary, and by a complex tectonic setting related to the intense Campi Flegrei volcanic activity. The northern part of the basin shows an inner shelf with maximum depth of 50 m, deepening to 100 m with gentle slopes and delimited by a belt of submarine volcanic edifices: starting from East, they are called Miseno Bank, Pentapalumbo Bank and Nisida Bank (see Figure 3A). The morphological investigations have revealed the presence of deposits in the deeper and flat part of the Gulf, especially around Miseno Bank and in the central part of the basin (areas in light brown, Figure 3A; Aiello et al., 2012). The seismic sections reported in the same publication evidence the presence of buried deposits with peculiar characteristics, which have been characterized and denoted as paleo-landslides. Figure 3B reports the profile along which they have been found, evidenced in red: one lies along the transect L69\_07, extending in the E-W direction and showing a potential deposit close to Nisida; the second refers to the line L74\_07, running in the N-S direction from Pozzuoli. The morphological evidence close to Miseno Bank and the two buried deposits found in the seismic profiles will be taken as the basis for the submarine landslide scenarios adopted for this investigation.

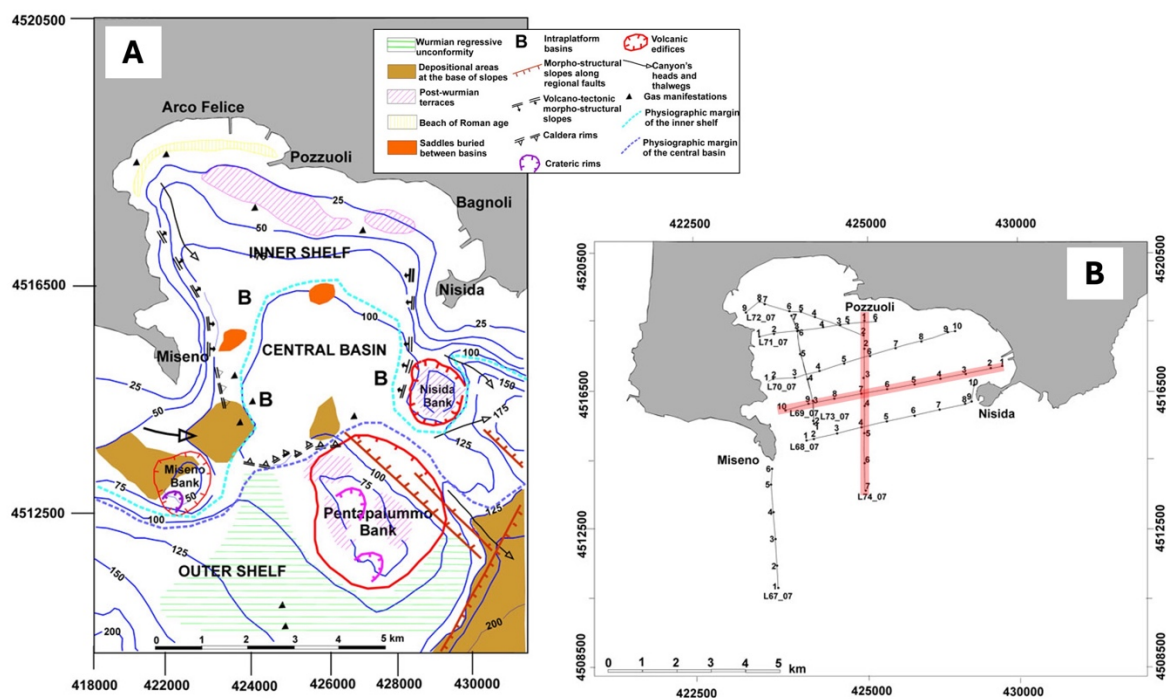




**Figure 3. Panel A) Sketch of the main morphological submarine features of the Gulf of Pozzuoli. Panel B) seismic lines acquired in the seismic survey illustrated in Aiello et al. (2012); the profiles with traces of paleo-landslides are evidenced in red. Figures modified from Aiello et al. (2012).**

As concerns subaerial sliding, a comprehensive geodatabase (CAFLAG) documents 2302 landslide events from 1828 to 2017, most of which consists of rock falls affecting volcanic slopes and rainfall-induced slides in pyroclastic deposits (Esposito and Matano, 2023). Landslide hazards affect over 15% of the subaerial Campi Flegrei area, with varying risk levels among towns (Calcaterra and di Martire, 2022). The events of interest here are the ones potentially interacting with water: the candidates are then restricted to collapses along the coastline that are not simple rockfalls (surely generating high waves but only locally, dissipating quickly), but more complex landslides involving a coherent mass impacting the water and moving along the seafloor.

Based on all these considerations, a set of four landslide scenarios has been arranged for the numerical simulations. Table 3 summarizes their geomorphological characteristics (volume, area, maximum thickness and initial elevation), while Figure 4 reports the position of the initial masses for each case. Three of them are submarine and cover different positions over the Gulf of Pozzuoli, while the fourth is subaerial.

Scenario 1 (blue contour in Figure 4) is located just south of Capo Miseno, at the western end of the Gulf, and has been reconstructed starting from the deposit shown in brown in Figure 3. The hypothesis is that the mass detached from the seafloor depression between Capo Miseno and the Miseno Bank, with the constraint to obtain a volume comparable to the observed deposit at the toe of the slope: since an accurate estimate of this does not exist, a conservative approach has been adopted, assuming a volume of almost 3 million m<sup>3</sup> for this scenario.

Scenario 2 (in magenta, Figure 4) lies in the central part of the Gulf and has been built based on the buried paleo-landslide recognized in the seismic profile just south of Pozzuoli (Figure 3). Its morphology is quite similar to Scenario 1, with volume and initial area slightly smaller, though its shape is more elongated in the sliding direction.

Scenario 3 (green boundary, Figure 4) is placed in the eastern part of the basin, and recalls a buried paleo-landslide as well, relative to another seismic transect (E-W from Nisida, see Figure 3). This scenario shows a slightly larger volume (around 4 million m<sup>3</sup>), a slightly larger initial thickness and moves from shallower water: all these elements suggest a higher capability of triggering relevant waves.

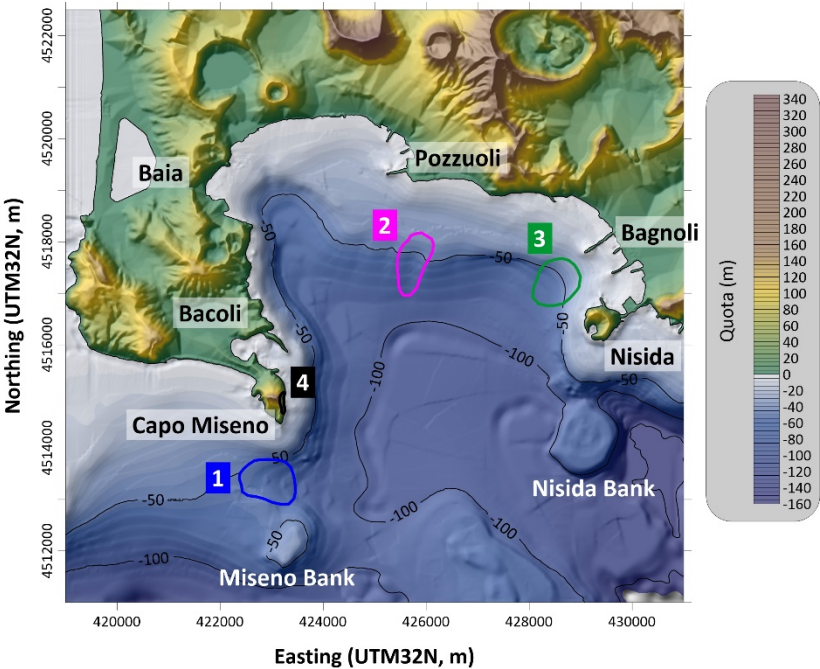
Scenario 4 (in black, Figure 4) is the only subaerial scenario, and is located along the coastal cliffs of Capo Miseno, at the western end of the Gulf of Pozzuoli. It has been chosen by morphological considerations, assuming the large coastal subaerial scar of the eastern flank of Capo Miseno - still visible now - originated from a single, sudden collapse. The resulting scenario is quite different from the other cases: volume much smaller (around half million m<sup>3</sup>) and much larger initial thickness (maximum of more than 50 m).

**Table 3. Morphological characteristics of the Gulf of Pozzuoli landslide scenarios.**



257

Scenario	Environment	Volume (10 <sup>6</sup> m <sup>3</sup> )	Area (km <sup>2</sup> )	Maximum Thickness (m)	Initial maximum elevation (m)
1	Submarine	2.98	0.77	9.47	-49
2	Submarine	2.30	0.56	10.11	-37
3	Submarine	4.12	0.63	12.73	-27
4	Subaerial	0.58	0.03	56.77	126



258

259 **Figure 4. Location of the initial bodies for the four landslide scenarios hypothesized: in blue, Scenario 1, between Capo Miseno and**  
260 **Miseno Bank; in magenta, Scenario 2, south of Pozzuoli; in green, Scenario 3, offshore Bagnoli; in black, Scenario 4, along the cliffs**  
261 **of Capo Miseno.**

262 **3.2 Landslide simulations**

263 The code UBO-BLOCK has been applied to each of the scenarios previously described. The software requires as input the  
264 initial landslide configuration (the undisturbed sliding surface and the upper surface of the mass), the predefined trajectory of  
265 the CoM and the lateral boundaries of the surface swept by the sliding motion. In this way it is possible to obtain the time  
266 history of the landslide shape changes and of its dynamics, representing the input for the computation of the tsunamigenic  
267 impulse.



3.2.1 Scenario 1

The first scenario is submarine, with a volume around 3 million m<sup>3</sup>, and is placed south of Capo Miseno. Figure 5A shows the initial thickness distribution (yellow-red scale), and the predefined trajectory for the CoM, that has been determined based on the position of the final deposit found from the geomorphological survey (dashed-blue boundary). Figure 5B reports a section of the landslide, taken along the CoM trajectory: as previously noticed, the slopes are quite gentle, with an average value of 1.5° for this case. In the simulation, the sliding mass settles between 80 and 100 m sea depth (red line, Figure 5B), reaching a maximum velocity of around 5 m/s after 200 seconds (Figure 5C), and decelerating quickly due to low seafloor gradient.

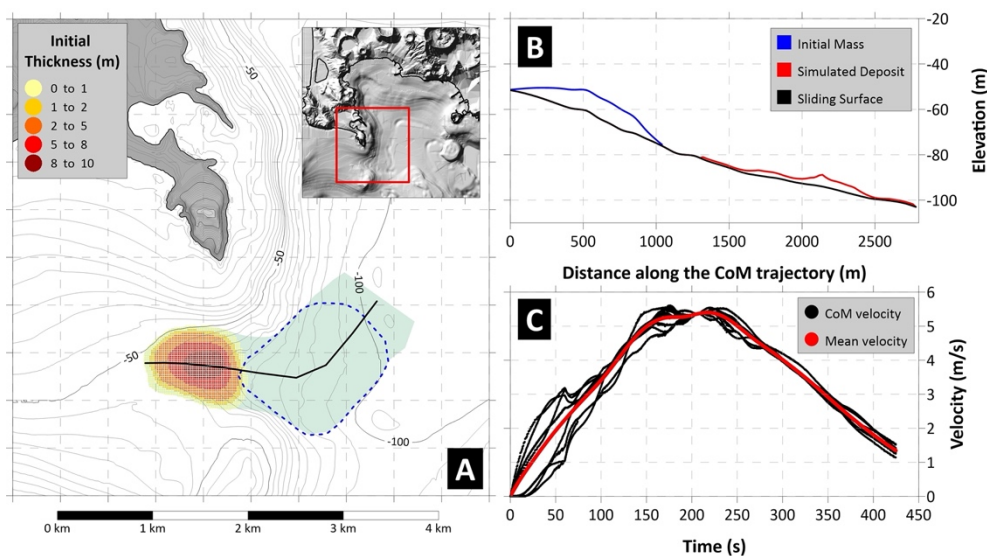
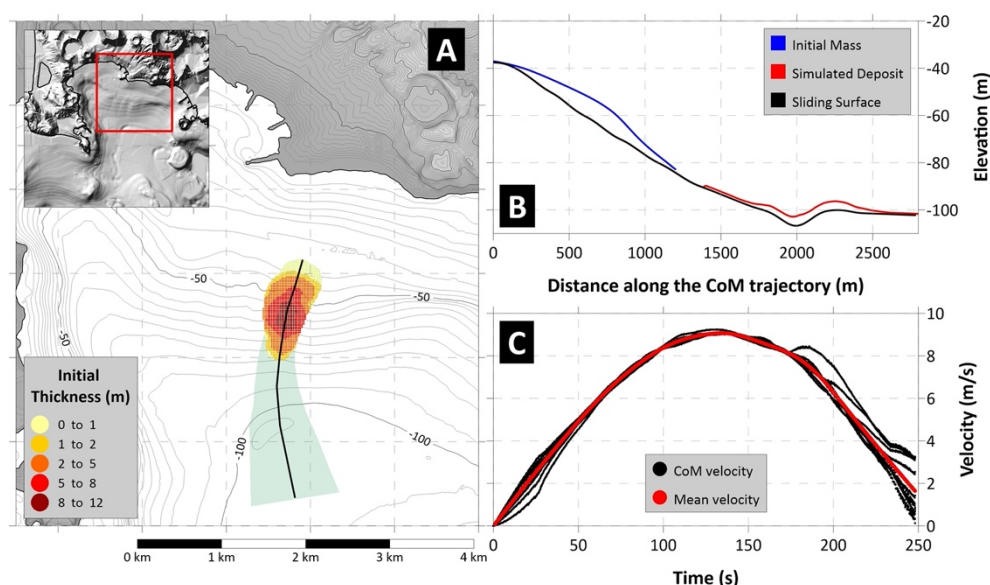


**Figure 5. Panel A) Map of the initial sliding mass for Scenario 1, with initial thickness shown by the yellow-red scale. The black line marks the CoM predefined trajectory, defined to fit the observed deposit (dashed-blue boundary). The area swept by the sliding motion is highlighted in green. Panel B) Landslide profile along the CoM trajectory: in black the undisturbed sliding surface; in blue the initial mass; in red the simulated deposit. Panel C) Sliding velocity time history: in red the average, in black the values for each CoM.**

3.2.2 Scenario 2

The second scenario is still submarine and is placed in the central part of the Gulf of Pozzuoli, about 1 km offshore from the piers of the homonymous city (Figure 6A). The hypothesized initial mass has been placed along the steeper slope connecting the shallow-water shelf to the deeper sea. The volume is similar to Scenario 1 (see Table 2), and the predefined sliding direction (black line in Figure 6A) mainly extends in the north-south direction. The simulation shows the deposit reaching the sub-horizontal seafloor at about 100 m depth (Figure 6B), with acceleration and deceleration phases almost symmetric, around the peak velocity value of 9 m/s (Figure 6C).



288

289 **Figure 6. Panel A) Map of the initial sliding mass for Scenario 2, with initial thickness shown by the yellow-red scale. The black line**  
 290 **marks the CoM predefined trajectory. The area swept by the sliding motion is highlighted in green. Panel B) Landslide profile along**  
 291 **the CoM trajectory: in black the undisturbed sliding surface; in blue the initial mass; in red the simulated deposit. Panel C) Sliding**  
 292 **velocity time history: in red the average, in black the values for each CoM.**

### 293 3.2.3 Scenario 3

294 The last submarine scenario is located on the eastern side of the basin, just north of the small peninsula of Nisida and few  
 295 hundreds of meters offshore Bagnoli (Figure 7A). As for the previous cases, the initial thickness is shown by the area in the  
 296 yellow-red scale, showing that the mass is not distributed uniformly, but with the thicker part placed in deeper water. The  
 297 sliding motion follows the main bathymetric gradient, south-westward (black line, Figure 7A), stopping at about 100 m depth,  
 298 where the slope is quite horizontal (Figure 7B). The dynamics is characterized by a shorter acceleration phase, reaching the  
 299 maximum velocity of almost 9 m/s after around 2 minutes (Figure 7C), followed by a longer deceleration taking 4 minutes  
 300 before stopping.



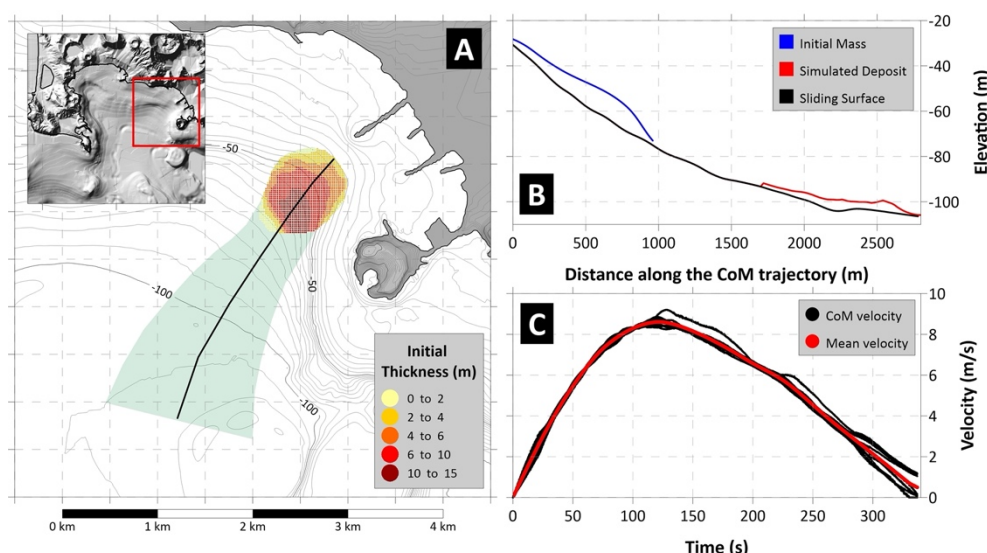


**Figure 7. Panel A) Map of the initial sliding mass for Scenario 3, with initial thickness shown by the yellow-red scale. The black line marks the CoM predefined trajectory. The area swept by the sliding motion is highlighted in green. Panel B) Landslide profile along the CoM trajectory: in black the undisturbed sliding surface; in blue the initial mass; in red the simulated deposit. Panel C) Sliding velocity time history: in red the average, in black the values for each CoM.**

### 3.2.4 Scenario 4

This scenario is the only subaerial one and presents very different morphological features compared to the previously illustrated cases: much smaller volume and initial area (see Table 2), much larger initial thickness, and an aspect ratio (length/width) very different from the submarine cases, as visible from Figure 8A. The initial mass has been hypothesized “filling” the subaerial, coastal scar still visible now along the eastern flank of Capo Miseno. Though purely theoretical, this type of collapse is not unusual in the whole area of the Gulf of Naples; this scenario can be considered an endmember for this category of landslides. The simulation shows that the deposit reaches a sub-horizontal area at 70-80 m depth (Figure 8B), with dynamics again different from the previous cases: a sudden acceleration brings the sliding mass at about 23 m/s within 10 seconds (Figure 8C), due to the very steep slope characterizing the first part of the trajectory (black line in Figure 8B); then the submarine shelf in very shallow water provokes an abrupt deceleration, down to 5 m/s, before a second acceleration due to the increasing slope between 20 and 60 m b.s.l., up to 10 m/s. Finally, the slide stops about 2 minutes after the onset.



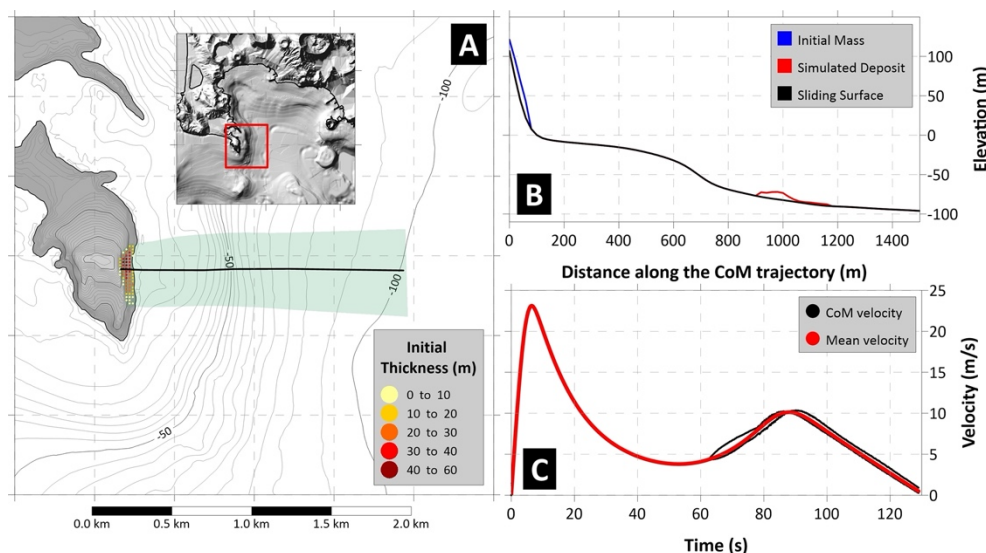


**Figure 8. Panel A) Map of the initial sliding mass for Scenario 4, with initial thickness shown by the yellow-red scale. The black line marks the CoM predefined trajectory. The area swept by the sliding motion is highlighted in green. Panel B) Landslide profile along the CoM trajectory: in black the undisturbed sliding surface; in blue the initial mass; in red the simulated deposit. Panel C) Sliding velocity time history: in red the average, in black the values for each CoM.**

### 3.3 Tsunami simulations

As illustrated previously, tsunamis can be significantly affected, during the propagation, by the hydrodynamic effect of dispersion, due to the different phase velocity characterizing its components. This phenomenon is particularly evident for short oscillations, which are more often induced by landslides. It is possible to estimate the distance at which such effects become predominant through Eq. (1), applying it to each of the studied scenarios. The dispersion can be quantified through the ratio  $\lambda/h$ , with  $\lambda$  tsunami wavelength and  $h$  sea depth that can be determined as follows:

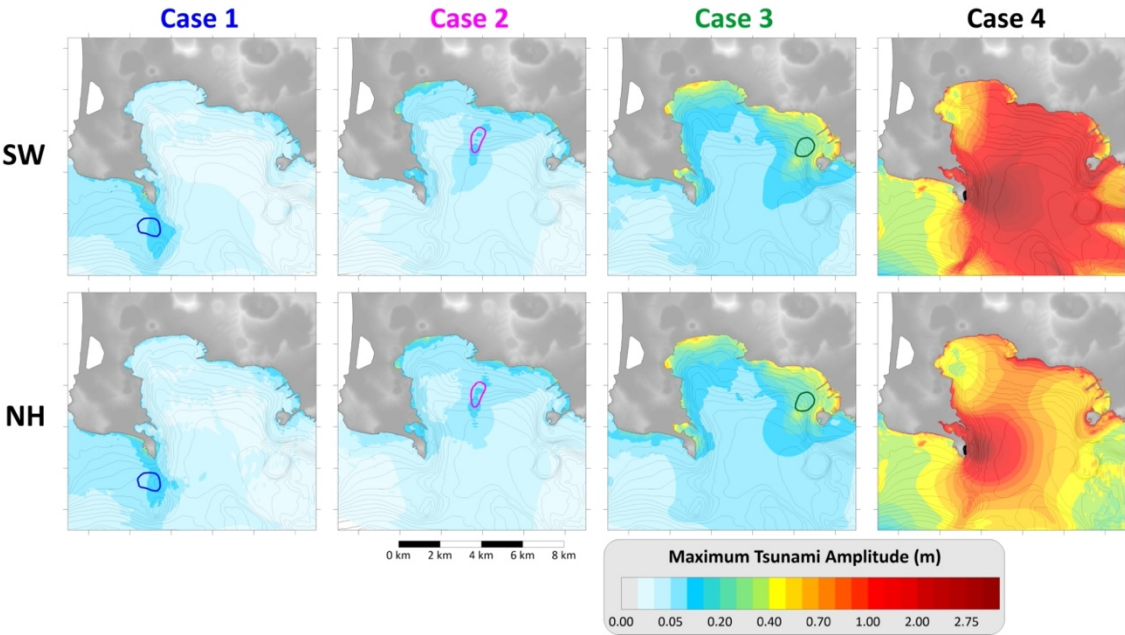
- $\lambda$ , the initial wavelength of the tsunami, can be assessed in a first approximation as twice the longitudinal length of the slide, called  $b$ . This assumption, adopted in Heidarzadeh et al. (2023), though quite simplistic and rough, provides a first reasonable indication for this quantity.
- Since the focus here goes to the minimum value for the ratio  $\lambda/h$ , delimiting the validity of SW approach, a value representing the maximum depth  $h$  for the tsunami propagation inside the Gulf of Pozzuoli is assumed: 105 m. The waves that are in the SW regime for this value, will satisfy this requirement also for shallower water.

Table 4 reports the estimations obtained for the landslide scenarios here adopted: the three submarine cases are in the SW regime, with the dispersion manifesting only for distances larger than the Gulf of Pozzuoli dimension. The subaerial case (Scenario 4) generates waves that are suddenly dominated by the dispersive effects: for this case the use of SW for the propagation on the whole Gulf of Pozzuoli seems not suitable.



**Table 4. Computation of the dispersion distance for the four scenarios here studied ( $b$  landslide length;  $\lambda$ : initial wavelength, assumed to coincide with  $b$ ;  $h$  water depth (fixed at 105 m);  $D$  dispersion distance, computed by Eq. (1);  $d$ : distance for which dispersion effects become predominant).**

Scenario	Environment	$b$ (m)	$\lambda/h$	$D$	$d$ (km)
1	Submarine	1090	20.7	10.7	11.7
2	Submarine	1260	24.0	14.4	18.1
3	Submarine	1010	19.2	9.2	9.3
4	Subaerial	170	3.24	0.26	0.05



**Figure 9. Maximum water amplitude on each node of the computational grid for the four scenarios considered: each of them are simulated through the shallow-water (SW) and the Boussinesq (NH) approach. The coloured boundaries report the initial position of the respective landslide source.**

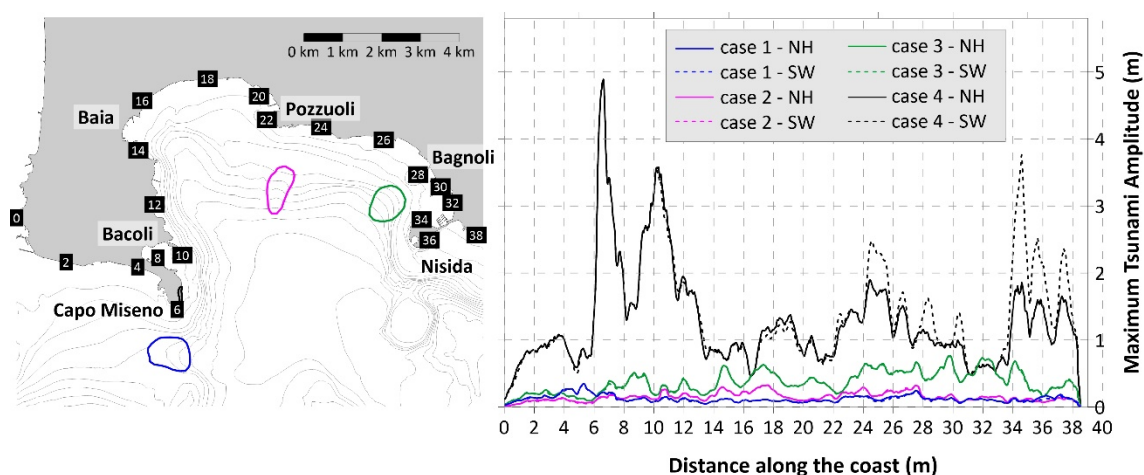
The simulations of the tsunamis generated by the sliding scenarios were performed using the JAGURS software, employing both the SW and the non-hydrostatic (NH) approaches, with the non-linear version of the equations in both cases. This strategy allows to investigate the suitability of the considerations previously made on the effects of dispersion on the tsunami propagation. Figure 9 illustrates the maximum water amplitude on each point of the computational domain for each scenario, comparing the two approaches: SW (upper row of plots) and NH (lower row). For the submarine scenarios (1, 2 and 3) the differences are negligible; for Case 4 (last column) significant differences are evident, with the NH approach showing much



353 more localized effects compared to SW. This confirms the earlier hypothesis that dispersion effects cannot be neglected for  
354 sources of this type.

355 From a hazard assessment perspective, submarine landslides generate relatively small tsunamis in the Gulf of Pozzuoli. In  
356 Cases 1 and 2, the maximum wave amplitudes are on the order of some tens of centimetres. In Case 3, the maximum amplitude  
357 exceeds 50 cm along the coastal stretch between Bagnoli and Nisida, which, while not catastrophic, could still cause damages  
358 to small boats and generate currents in smaller sub-basins. In contrast, Case 4 produces more significant waves, especially at  
359 the local scale. Although the NH simulations show a rapid damping, localized amplifications can be observed in more distant  
360 coastal stretches, such as around Pozzuoli (northern coast) and the Nisida peninsula (on the east).

361 Figure 10 depicts the maximum tsunami amplitude along the coast vs the cumulative coastal distance, measured from the  
362 eastern extreme of the computational domain and represented with the black labels, in the left plot. The SW-NH simulations  
363 are almost indistinguishable for the three submarine scenarios (right plot in Figure 10), with the respective waves amplitude  
364 that are almost superimposed. Cases 1 and 2 show limited effects on the coast, while Case 3 generates maximum amplitudes  
365 of over 0.5 m between Pozzuoli and Nisida. As previously observed, on the contrary, for the subaerial case (Scenario 4) the  
366 dispersive effects play a key role, lowering considerably the maximum amplitude at the coast starting from the Pozzuoli coastal  
367 stretch (around 20 km of cumulative distance along the coast), with values almost halved at the opposite side of the Gulf.  
368 Conversely, the two approaches produce similar waves for coastal stretches closer to the source, since for these the tsunami  
369 travels in shallower water and the dispersive effects are then less impacting. As already observed, this scenario produces the  
370 most impacting tsunami, with peak value close to 5 m in Capo Miseno and local amplifications at Pozzuoli and Nisida with  
371 amplitudes of almost 2 m.



372

373 **Figure 10.** The map on the left reports the initial boundaries of the landslide scenarios. The cumulative distance along the coast is  
374 measured from the eastern extreme of the computational domain. The plot on the right depicts the maximum water amplitude along  
375 the coast for the four scenarios, with comparison between NH (continuous lines) and SW (dashed lines).



Figure 11 depicts the sketches of the first minutes of propagation for each scenario: all simulations show the typical feature characterizing landslide-tsunamis, the almost circular shape of the tsunami signal, mimicking a point-like source. This polar symmetry is lost when the wave interacts with shallow water and non-linear effects become predominant. A positive front (yellow-red scale, meaning sea level increase) propagates in the same direction of the sliding motion, while a negative one (cyan-blue scale) moves in the opposite side. For cases 2 and 3, the first manifestation of the tsunami at the coastal stretch close to the source - presumably affected by the larger waves - is a negative signal, meaning that the water withdraws and is followed later by a sea level increase: in terms of early warning this is an undoubted advantage, since it can act as a precursor of an upcoming flooding. For case 1 the situation is different, since the slide motion does not have a direction opposite to the dryland: a positive front enters the Gulf of Pozzuoli, while a negative one moves west of Capo Miseno, to the coastal stretch out of the basin. As to case 4, the sliding motion starts in the subaerial environment, resulting into an always positive tsunami front. Notice also the sequence of high frequency waves characterizing this scenario, especially evident in the 3- and 4-minutes sketches (last row of plots), reflecting the smaller spatial dimensions of the tsunami source.

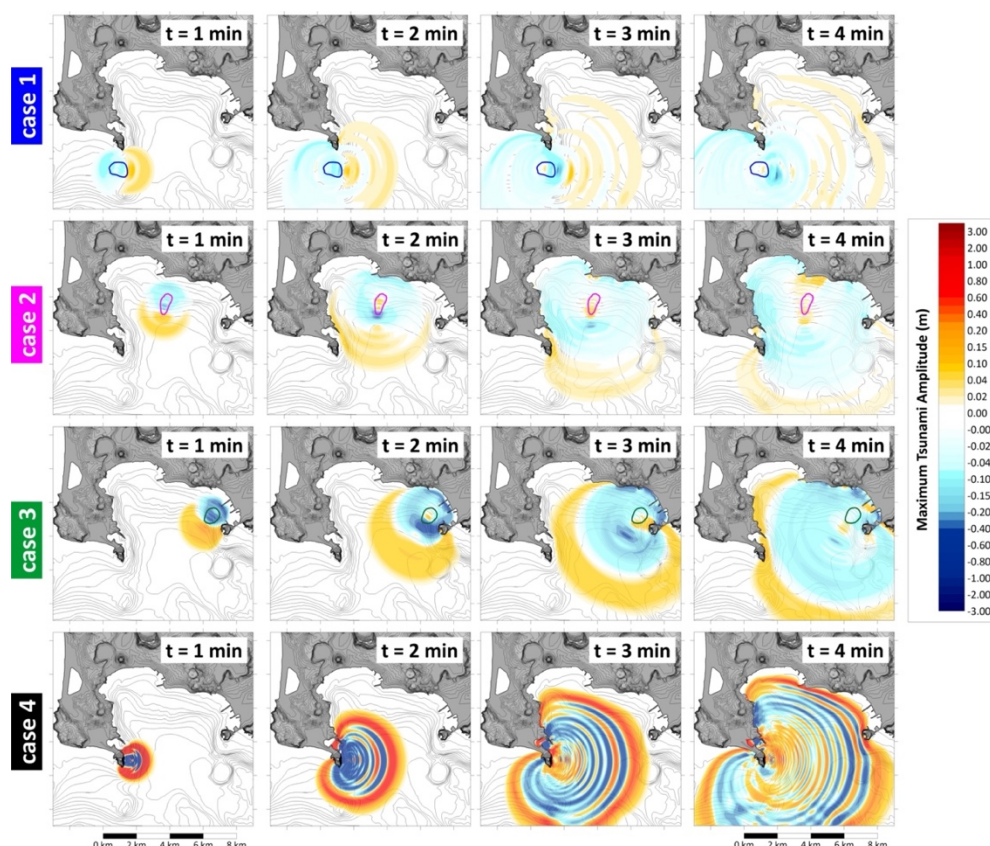
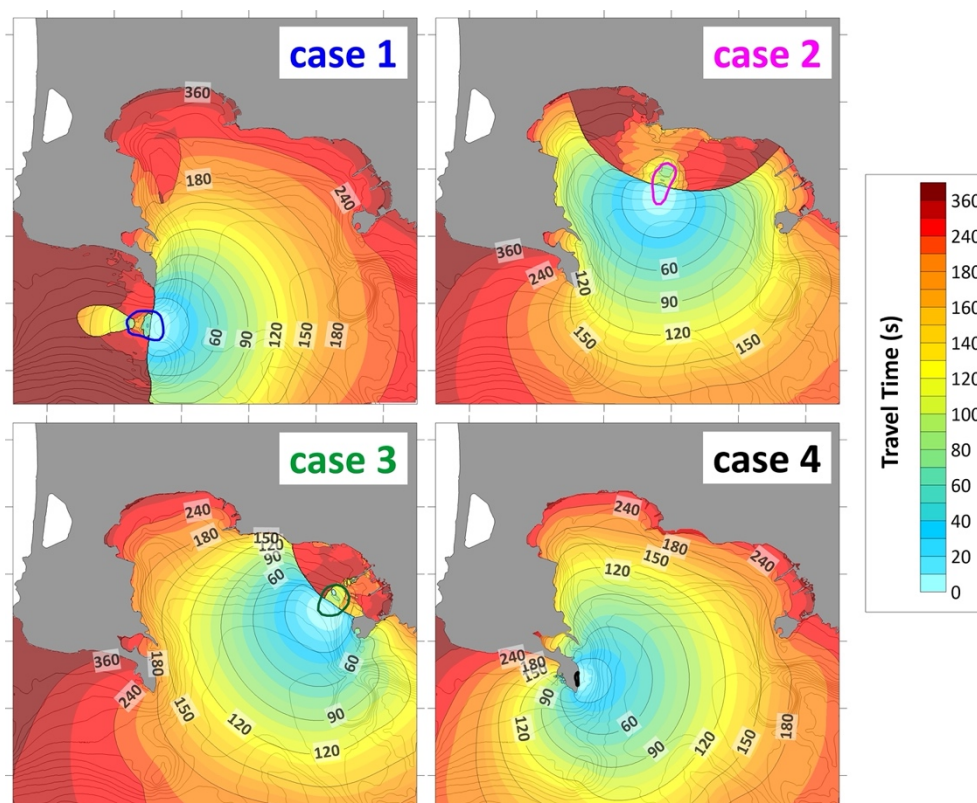


Figure 11. Propagation sketches at 1 minute intervals of the four landslide-tsunami scenarios investigated (NH approach). The yellow-red scale marks the positive values (sea level increase), the cyan-blue scale is for negative ones (sea level sinking). The coloured contours represent the respective initial landslide boundary.





In all cases represented in Figure 11, the tsunami affects most of the Gulf of Pozzuoli coasts within 4 minutes. Figure 12 reports the travel time for each point of the computational domain, providing precious insights from the warning point of view: independently from the initial position, the waves take approximately 3 to 6 minutes to affect all the coasts of the basin. Case 2 is the fastest, also due to its position at the centre of the Gulf. The north-western coastal stretch, on the contrary, is the one reached latest (5 to 6 minutes) in every scenario: the waves are slowed down by the shallow-water shelf that in this area is particularly large, compared to the other areas (as confirmed by the morphology, Figure 4). It is worth to specify that the code JAGURS registers the first positive signal for each computational cell: this explains the anomalous pattern of the tsunami opposite to the slide direction, particularly evident in Case 1 (westward, upper left panel, Figure 12) and Case 2 (northward, upper right panel).



**Figure 12. Travel time, in seconds, of the tsunamis generated by the four landslide scenarios here hypothesized. The position of the initial mass is marked by the respective coloured boundaries.**

## 4 Discussion

The numerical simulations illustrated in the previous section provide some precious insights about the tsunami hazard pattern within the Gulf of Pozzuoli. Submarine collapses of the size adopted in this study generate waves that do not represent a threat for coastal population, but which can damage small boats, which are present in a great number within the Gulf of Pozzuoli.



409 Conversely, the subaerial scenario produces high waves especially in the near field (almost 5 meters high), which rapidly  
410 attenuate with distance thanks to dispersive effects. Some distant coastal stretches are affected by local amplifications, with  
411 maximum amplitudes reaching almost 2 m (Pozzuoli, Nisida), highlighting the need to investigate this type of events. In most  
412 cases, the tsunami reaches the shoreline in a few minutes with a positive signal, meaning that it manifests as a water level  
413 increase. Only in limited coastal stretches, and not for all scenarios, the first signal is negative, i.e. the sea withdraws for some  
414 minutes, providing a crucial precursor of an incoming wave in terms of early warning. In a few words, these events can occur  
415 totally unannounced, reflecting the definition of “surprise tsunamis” given in Ward (2001). In the following, some specific  
416 issues arising from the approach adopted and the simulation results are discussed.

417 *Landslide scenarios.* The scenario approach here adopted is a consequence of the lack of knowledge about the underwater  
418 landslide bodies in the Gulf of Pozzuoli. Geophysical and bathymetric surveys have evidenced the presence of some ancient  
419 collapses, buried by the sediments, in the deeper part of the basin at the toe of the slopes, but a general pattern of mass transport  
420 processes in the Gulf of Pozzuoli, with recurrence time and volume estimation, doesn’t exist. The sources adopted have been  
421 reconstructed based on the pieces of evidence found in the scientific literature and on geomorphological considerations (margin  
422 slopes, existing scars, basin depth), assuming that they are representative of the maximum credible occurrences expected in  
423 the area. As a result, three submarine masses have been reconstructed, with similar volumes (few million m<sup>3</sup>), thickness (a  
424 maximum of about ten meters) and detachment depth (in shallow water, between 30 and 50 m). The fourth case is a coastal  
425 subaerial collapse and is characterized by a very different morphology: it can be considered as the endmember of this type of  
426 landslide, since no direct evidence exists of bigger collapses interacting with the sea. These scenarios cover the whole extent  
427 of the Gulf, providing then a general idea of the impact expected from the ensuing tsunamis. However, larger collapses can’t  
428 be ruled out, especially in case of intensification of the Campi Flegrei volcanic activity providing possible triggers and, in the  
429 long term, slope oversteepening.

430 *Dispersion effects.* For tsunamis of non-seismic origin, the effect of dispersion should be always taken into consideration, since  
431 it can change consistently the propagation pattern with respect to the classic SW approach. The discrepancy grows with the  
432 distance from the source, depending on the wavelength of the initial signal and on the depth of the basin where the perturbation  
433 propagates. Eq. (1) provided rough estimates of this distance for the scenarios considered (reported in Table 4), suggesting  
434 that for the submarine cases the dispersion is negligible within the Gulf of Pozzuoli domain. Numerical simulations confirmed  
435 this hypothesis: the application of the code with (NH) and without (SW) dispersion produced almost identical tsunamis,  
436 proving that the simpler and faster approach is sufficient to assess properly the tsunami hazard for these cases. For the subaerial  
437 case, on the contrary, the difference is marked, as evidenced in Figure 10 by the maximum amplitudes along the coast. The  
438 modelling effort, then, should consider the morphological features of the source generating the tsunami, keeping in mind that  
439 subaerial masses collapsing into the sea usually generate shorter perturbations. In these cases, dispersive effects can become  
440 relevant even for brief distances, and the application of the SW approach could produce an overestimation of the tsunami  
441 impact on the coasts.





442 *Coastal and non-linear phenomena.* From the propagation plots (Figure 11) it is possible to infer some peculiar features of the  
443 tsunami close to the coast, where the interaction with shallow water and minor basins can induce non-linear effects. For  
444 example, for case 2 a positive signal propagating in the Bacoli Bay - a minor inlet just north of Capo Miseno on the western  
445 part of the Gulf (see also Figure 13 for location) - can be noticed, evident especially in the  $t = 3$  and 4 minutes sketches. This  
446 is visible, while less marked, also for the other scenarios, and suggests the possibility of the excitation of the normal modes of  
447 this sub-basin by the tsunami: this phenomenon, known as resonance, can occur for every basin affected by an external  
448 perturbation, and is for example the mechanism at the basis of the generation of the meteotsunamis (Vilibic et al., 2016). The  
449 morphology of the basin determines the periods of the resonant modes typical of the basin. Rabinovich (2009) obtained a set  
450 of simple expressions allowing to estimate them for basic geometries. For example, for a rectangular basin of length  $L$  and  
451 uniform depth  $h$ , the period  $T$  of the fundamental mode is:

$$452 \quad T = \frac{2L}{\sqrt{gh}} \quad (2)$$

453 where  $g$  is the gravitational acceleration. Focusing on the Bacoli Bay case, Figure 13 reports the marigrams obtained from two  
454 virtual tide gauges placed inside the inlet (tg#1, in red) and at its mouth (tg#2, in black), depicting the two respective time  
455 histories in the four scenarios considered. The comparison of the signals shows clearly, for Cases 1, 2 and 3, that inside the  
456 bay the perturbations behave as standing waves, characterized by regular oscillations lasting for at least 30 minutes (final  
457 simulation time) with an approximate period of 200 s and evident amplifications if compared to the oscillations out of the basin  
458 (in black). The tsunami generated by Case 3, in particular, is amplified five times with respect to the incoming signal. Assuming  
459 for the Bacoli Bay a simplified rectangular geometry ( $L \approx 1000$  m,  $h \approx 10$  m) and applying Eq. (2), one can estimate the  
460 fundamental mode as  $T \approx 200$  s, in full agreement with the features deduced from the virtual tide gauges. Moreover, the  
461 subaerial scenario (Case 4) is less subject to the amplification when entering the inlet compared to the other cases, due to the  
462 shorter period characterizing its oscillations.

463

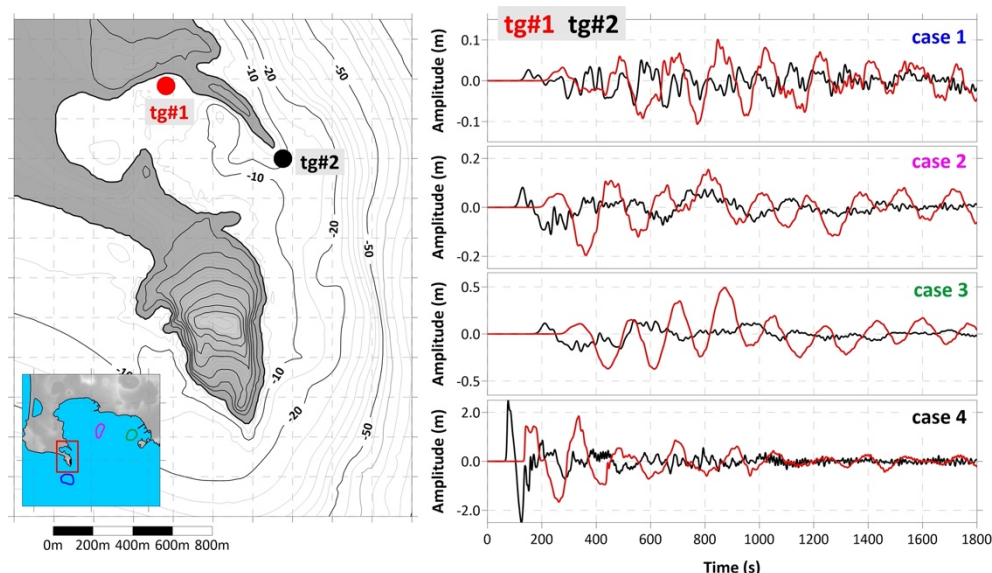


**Figure 13. Virtual tide gauges at the entrance (in black) and inside (in red) the Bacoli Bay. On the left, their location; on the right, the comparison between the marigrams for the scenarios here simulated.**

## 5 Conclusions

The Gulf of Pozzuoli covers a significant portion of the Campi Flegrei caldera, a region of significant geological and volcanic activity. Intense seismic and volcanic processes have the potential to destabilize large sliding bodies both in the subaerial and in the submarine environment. When these masses interact with the water, they can generate tsunamis that may impact the entire basin's coastline, posing potential risks to local communities, coastal infrastructures, and marine activities.

Despite the region being the object of extensive geological and geophysical investigations, a comprehensive understanding of mass transport processes remains limited. A scenario-based approach is then adopted, analysing four representative cases, based on the limited geological evidence and on morphological considerations: three submarine bodies, with similar volume (few million  $\text{m}^3$ , occurring in shallow water) and one subaerial slide (smaller mass, occurring on the coastline). These scenarios, though not reproducing actual occurrences, provide precious insights into the potential tsunami generation mechanisms and their subsequent impact on coastal areas, providing an important basis for possible risk mitigation strategies. The sliding dynamics and the resulting tsunamis are simulated using numerical techniques that account for key hydrodynamic phenomena such as dispersion, nonlinear coastal effects, and resonance.

The simulations results indicate that submarine landslides generally produce waves of limited amplitude on the coast, with a maximum height of 0.5 meters, as observed for case 3. While these tsunamis do not represent a major threat to coastal communities, they could still cause localized damages, for example to small boats moored in the harbours across the Gulf of Pozzuoli. Furthermore, resonance effects in smaller basins, such as harbours, can amplify an incoming wave, preventing its dissipation and resulting in standing wave affecting the coast for long time: simulation outcomes show that in the Bacoli Bay



485 - placed in the western sector of the gulf – the incoming signal is amplified up to five times, with a sequence of regular  
486 oscillations with a period of 200 s, affecting the basin for at least 30 minutes, which reflects the normal modes typical of the  
487 inlet. This can repeat in every coastal basin, each one characterized by its own geometry and fundamental mode and is worthy  
488 of specific and detailed investigation. In contrast, the subaerial slide scenario results in significantly larger waves, exceeding  
489 4 meters close to the source. The tsunami amplitude dampens rapidly with distance, due to dispersion, but in some coastal  
490 stretches, Pozzuoli on the north and Nisida on the east, it reaches almost 2 meters.

491 The investigation here presented highlights the complex interplay between geological processes, hydrodynamic phenomena,  
492 and coastal hazard in the Gulf of Pozzuoli. The results emphasize the need for detailed study and monitoring of potential  
493 unstable masses, especially in coastal subaerial environment where they can give rise to large tsunamis threatening the whole  
494 Gulf of Pozzuoli, and for risk management strategies to mitigate the potential impact of tsunamis in this active volcanic region.

#### 495 **Code availability**

496 The numerical codes UBO-BLOCK and UBO-TSUIIMP for landslide dynamics and tsunamigenic impulse computation  
497 respectively are available under request to the authors; the code JAGURS can be freely downloaded from the link:  
498 <https://github.com/jagurs-admin/jagurs>.

#### 499 **Data availability**

500 The computational grids have been obtained from the elaboration of raw datasets available online, which have been  
501 interpolated and readjusted. They are available under request to the authors.

#### 502 **Author contribution**

503 FZ and AA conceptualized the investigation; FZ, CA and MZ prepared the computational grids and the landslide scenario  
504 datasets; FZ and LS performed the simulations; FZ prepared the manuscript, with the contribution from all co-authors; FZ and  
505 AA supervised the whole manuscript realization.

#### 506 **Competing interests**

507 The authors declare that they have no conflict of interest.



## 508 Acknowledgements

509 The authors are grateful to Prof. Jacopo Selva, University of Naples, Federico II, for the productive discussion about the  
510 potential tsunami sources in the Gulf of Pozzuoli related to the Campi Flegrei activity.

## 511 References

- 512 Aiello, G., Marsella, E. and Fiore, V. D.: New seismo-stratigraphic and marine magnetic data of the Gulf of Pozzuoli (Naples  
513 Bay, Tyrrhenian Sea, Italy): inferences for the tectonic and magmatic events of the Phlegrean Fields volcanic complex  
514 (Campania), *Mar Geophys Res*, 33, 97–125, <https://doi.org/10.1007/s11001-012-9150-8>, 2012.
- 515 Aiello, G., Giordano, L. and Giordano, F.: High-resolution seismic stratigraphy of the Gulf of Pozzuoli (Naples Bay) and  
516 relationships with submarine volcanic setting of the Phlegrean Fields volcanic complex, *Rend. Fis. Acc. Lincei*, 27, 775–801,  
517 <https://doi.org/10.1007/s12210-016-0573-z>, 2016.
- 518 Baba, T., Ando, K., Matsuoka, D., Hyodo, M., Hori, T., Takahashi, N., Obayashi, R., Imato, Y., Kitamura, D., Uehara, H.,  
519 Kato, T. and Saka, R.: Large-scale, highspeed tsunami prediction for the Great Nankai Trough Earthquake on the K computer,  
520 *Intern Jour of High Per Comp App*, 30, doi: 10.1177/1094342015584090, 2015.
- 521 Behrens, J., Løvholt, F., Jalayer, F., Lorito, S., Salgado-Gálvez, M. A., Sørensen, M., Abadie, S., Aguirre-Ayerbe, I., Aniel-  
522 Quiroga, I., Babeyko, A., Baiguera, M., Basili, R., Belliazzi, S., Grezio, A., Johnson, K., Murphy, S., Paris, R., Rafliana, I.,  
523 De Risi, R., Rossetto, T., Selva, J., Taroni, M., Del Zoppo, M., Armigliato, A., Bureš, V., Cech, P., Cecioni, C.,  
524 Christodoulides, P., Davies, G., Dias, F., Bayraktar, H. B., González, M., Gritsevich, M., Guillas, S., Harbitz, C. B., Kânoğlu,  
525 U., Macías, J., Papadopoulos, G. A., Polet, J., Romano, F., Salamon, A., Scala, A., Stepinac, M., Tappin, D. R., Thio, H. K.,  
526 Tonini, R., Triantafyllou, I., Ulrich, T., Varini, E., Volpe, M. and Vyhmeister, E.: Probabilistic Tsunami Hazard and Risk  
527 Analysis: A Review of Research Gaps, *Front. Earth Sci*, 9:628772, doi: 10.3389/feart.2021.628772, 2021.
- 528 Bevilacqua, A., Isaia, R., Neri, A., Vitale, S., Aspinall, W. P., Bisson, M., Flandoli, F., Baxter, P. J., Bertagnini, A., Esposti  
529 Ongaro, T., Iannuzzi, E., Pistolesi, M. and Rosi, M.: Quantifying volcanic hazard at Campi Flegrei caldera (Italy) with  
530 uncertainty assessment: 1. Vent opening maps, *Journal of Geophysical Research: Solid Earth*, 120(4), 2309–2329.  
531 <https://doi.org/10.1002/2014JB011775>, 2015.
- 532 Calcaterra, D. and Di Martire, D.: Landslide Hazard and Risk in the Campi Flegrei Caldera, Italy. In: Orsi, G., D'Antonio, M.,  
533 Civetta, L. (eds) *Campi Flegrei. Active Volcanoes of the World*, Springer, Berlin, Heidelberg, [https://doi.org/10.1007/978-3-642-37060-1\\_13](https://doi.org/10.1007/978-3-642-37060-1_13), 2022.
- 535 Danesi, S., Pino, N. A., Carlino, S. and Kilburn, C. R.: Evolution in unrest processes at Campi Flegrei caldera as inferred from  
536 local seismicity, *Earth and Planetary Science Letters*, 626, 118530, doi: <https://doi.org/10.1016/j.epsl.2023.118530>, 2024.



- 537 De Natale, G., Troise, C., Pingue, F., Mastrolorenzo, G., Pappalardo, L., Battaglia, M. and Boschi, E.: The Campi Flegrei  
538 caldera: unrest mechanisms and hazards. In Troise, C., De Natale, G., Kilburn C. R. J. (eds), Mechanisms of Activity and  
539 Unrest at Large Calderas, Geological Society, London, Special Publications, <https://doi.org/10.1144/GSL.SP.2006.269.01.03>,  
540 2006.
- 541 De Ritis, R., Cocchi, L., Passaro, S. and Chiappini, M.: Giant landslide, hidden caldera structure, magnetic anomalies and  
542 tectonics in southern Tyrrhenian Sea (Italy), Geomorphology, 466, 109445, <https://doi.org/10.1016/j.geomorph.2024.109445>,  
543 2024.
- 544 De Vivo, B., Rolandi, G., Gans, P. B., Calvert, A., Bohrsen, W. A., Spera, F. J. and Belkin, H. E.: New constraints on the  
545 pyroclastic eruptive history of the Campanian volcanic Plain (Italy), Mineralogy and Petrology, 73, 47-65,  
546 <https://doi.org/10.1007/s007100170010>, 2001.
- 547 De Vivo, B., Belkin, H. E. and Rolandi, G.: Introduction to Vesuvius, Campi Flegrei, and Campanian Volcanism. In: De Vivo,  
548 B., Belkin, H. E., Rolandi, G. (eds) Vesuvius, Campi Flegrei, and Campanian Volcanism, Elsevier,  
549 <https://doi.org/10.1016/B978-0-12-816454-9.00001-8>, 2020.
- 550 Del Gaudio, C., Aquini, I., Ricciardi G. P., Ricco, C. and Scandone R.: Unrest episodes at Campi Flegrei: A reconstruction of  
551 vertical ground movements during 1905–2009, Journal of Volcanology and Geothermal Research, 195,10,  
552 <https://doi.org/10.1016/j.jvolgeores.2010.05.014>, 2010.
- 553 Di Vito, M., Acocella, V., Aiello, G., Barra, D., Battaglia, M., Carandente A., Del Gaudio C., de Vita, S., Ricciardi, G. P.,  
554 Ricco, C., Scandone, R. and Terrasi, F.: Magma transfer at Campi Flegrei caldera (Italy) before the 1538 AD eruption, Sci  
555 Rep, 6, 32245, <https://doi.org/10.1038/srep32245>, 2016.
- 556 DPC (Dipartimento della Protezione Civile - Civil Protection Department, Italy), MaGIC - Marine Geohazards along the Italian  
557 Coasts, <https://github.com/pcm-dpc/MaGIC>, last access 18 May 2023.
- 558 Ehara, A., Salmanidou, D. M., Heidarzadeh, M. and Guillas, S.: Multi-level emulation of tsunami simulations over Cilacap,  
559 South Java, Indonesia, Computational Geosciences, 27(1), 127-142, <https://doi.org/10.1007/s10596-022-10183-1>, 2023.
- 560 Esposito, G. and Matano, F.: A geodatabase of historical landslide events occurring in the highly urbanized volcanic area of  
561 Campi Flegrei, Italy, Earth Syst. Sci. Data, 15, 1133–1149, <https://doi.org/10.5194/essd-15-1133-2023>, 2023.
- 562 Gallotti, G., Zaniboni, F., Arcangeli, D., Angeli, C., Armigliato, A., Cocchi, L., Muccini, F., Zanetti, M., Tinti, S. and Ventura,  
563 G.: The tsunamigenic potential of landslide-generated tsunamis on the Vavilov seamount, Journal of Volcanology and  
564 Geothermal Research, 434, 107745, <https://doi.org/10.1016/j.jvolgeores.2023.107745>, 2023.



- 565 Gallotti, G., Zaniboni, F., Pagnoni, G., Romagnoli, C., Gamberi, F., Marani, M. and Tinti, S.: Tsunamis from prospected mass  
566 failure on the Marsili submarine volcano flanks and hints for tsunami hazard evaluation, *Bulletin of Volcanology*, 83, 2,  
567 <https://doi.org/10.1007/s00445-020-01425-0>, 2021.
- 568 Gasperini, L., Zaniboni, F., Armigliato, A., Tinti, S., Pagnoni, G., Özeren, M. S., Ligi, M., Natali, F. and Polonia, A.: Tsunami  
569 potential source in the eastern Sea of Marmara (NW Turkey), along the North Anatolian Fault system, *Landslides*, 19, 2295–  
570 2310, doi: 10.1007/s10346-022-01929-0, 2022.
- 571 Glimsdal, S., Pedersen, G., Harbitz, C. B. and Løvholt, F.: Dispersion of tsunamis: does it really matter?, *Nat. Hazards Earth*  
572 *Syst. Sci.*, 13, 1507–1526, doi: 10.5194/nhess-13-1507-2013, 2013.
- 573 Grezio, A., Cinti, F. R., Costa, A., Faenza, L., Perfetti, P., Pierdominici, S., Pondrelli, S., Sandri, L., Tierz, P., Tonini, R. and  
574 Selva, J.: Multisource Bayesian probabilistic tsunami hazard analysis for the Gulf of Naples (Italy), *Journal of Geophysical*  
575 *Research: Oceans*, 125, 2, <https://doi.org/10.1029/2019JC015373>, 2020.
- 576 Heidarzadeh, M., Gusman, A.R. and Mulia, I.E.: The landslide source of the eastern Mediterranean tsunami on 6 February  
577 2023 following the  $M_w$  7.8 Kahramanmaraş (Türkiye) inland earthquake, *Geosci. Lett.*, 10, 50, [https://doi.org/10.1186/s40562-](https://doi.org/10.1186/s40562-023-00304-8)  
578 [023-00304-8](https://doi.org/10.1186/s40562-023-00304-8), 2023.
- 579 Isaia, R., Di Giuseppe, M. G., Natale, J., Tramparulo, F. D. A., Troiano, A. and Vitale, S.: Volcano-tectonic setting of the  
580 Pisciarelli fumarole field, Campi Flegrei caldera, southern Italy: insights into fluid circulation patterns and hazard scenarios,  
581 *Tectonics*, 40, 5, <https://doi.org/10.1029/2020TC006227>, 2021.
- 582 Løvholt, F., Pedersen, G., Harbitz, C. B., Glimsdal, S. and Kim, J.: On the characteristics of landslide tsunamis, *Phil. Trans.*  
583 *R. Soc. A*, 373: 20140376, doi: 10.1098/rsta.2014.0376, 2015.
- 584 Mayer, K., Scheu, B., Montanaro, C., Yilmaz, T. I., Isaia, R., Aßbichler, D. and Dingwell, D. B.: Hydrothermal alteration of  
585 surficial rocks at Solfatara (Campi Flegrei): Petrophysical properties and implications for phreatic eruption processes, *Journal*  
586 *of Volcanology and Geothermal Research*, 320, 128-143, <https://doi.org/10.1016/j.jvolgeores.2016.04.020>, 2016.
- 587 Neri, A., Bevilacqua, A., Esposti Ongaro, T., Isaia, R., Aspinall, W. P., Bisson, M., Flandoli, F., Baxter P. J., Bertagnini, A.,  
588 Iannuzzi, E., Orsucci, S., Pistolesi, M., Rosi, M. and Vitale, S.: Quantifying volcanic hazard at Campi Flegrei caldera (Italy)  
589 with uncertainty assessment: 2. Pyroclastic density current invasion maps, *Journal of Geophysical Research: Solid Earth*, 120,  
590 4, 2330-2349, <https://doi.org/10.1002/2014JB011776>, 2015.
- 591 Paris, R., Ulvrová, M., Selva, J., Brizuela, B., Costa, A., Grezio, A., Lorito, S. and Tonini, R.: Probabilistic hazard analysis for  
592 tsunamis generated by subaqueous volcanic explosions in the Campi Flegrei caldera, Italy. *Journal of Volcanology and*  
593 *Geothermal Research*, 379, 106-116, <https://doi.org/10.1016/j.jvolgeores.2019.05.010>, 2019.





- 594 Perrotta, A., Scarpato, C., Luongo, G. and Morra, V.: The Campi Flegrei caldera boundary in the city of Naples. In: De Vivo,  
595 B. (ed.), *Developments in Volcanology*, Elsevier, Volume 9, 85-96, [https://doi.org/10.1016/S1871-644X\(06\)80019-7](https://doi.org/10.1016/S1871-644X(06)80019-7), 2006.
- 596 Rabinovich, B. A.: *Seiches and Harbor Oscillations*, Handbook of Coastal and Ocean Engineering, 93-236, 2009.
- 597 Ren, Z., Hou, J., Wang, P. and Wang, Y.: Tsunami resonance and standing waves in Hangzhou Bay, *Physics of Fluids*, 33, 8,  
598 <https://doi.org/10.1063/5.0059383>, 2021.
- 599 Rosi, M., Sbrana, A. and Principe, C.: The Phlegraean Fields: structural evolution, volcanic history and eruptive  
600 mechanisms, *Journal of Volcanology and Geothermal Research*, 17, 1-4, 273-288, [https://doi.org/10.1016/0377-](https://doi.org/10.1016/0377-0273(83)90072-0)  
601 [0273\(83\)90072-0](https://doi.org/10.1016/0377-0273(83)90072-0), 1983.
- 602 Sabino, L., *Analisi della pericolosità da tsunami generati da frana nell'area del Golfo di Pozzuoli e dei Campi Flegrei*, Second  
603 Level Degree in Physics of the Earth System, discussed on 14 march 2024, 2024 (in italian).
- 604 Saito, T.: *Tsunami Generation and Propagation*, 265 - Springer Geophysics, <https://doi.org/10.1007/978-4-431-56850-6>,  
605 2019.
- 606 Selva, J., Amato, A., Armigliato, A., Basili, R., Bernardi, F., Brizuela, B., Cerminara, M., de' Micheli Vitturi, M., Di Bucci,  
607 D., Di Manna, P., Esposti Ongaro, T., Lacanna, G., Lorito, S., Løvholt, F., Mangione, D., Panunzi, E., Piatanesi, A., Ricciardi,  
608 A., Ripepe, M., Romano, F., Santini, M., Scalzo, A., Tonini, R., Volpe, M. and Zaniboni, F.: Tsunami risk management for  
609 crustal earthquakes and non-seismic sources in Italy, *Riv. Nuovo Cim.*, 44, 69-144, [https://doi.org/10.1007/s40766-021-](https://doi.org/10.1007/s40766-021-00016-9)  
610 [00016-9](https://doi.org/10.1007/s40766-021-00016-9), 2021.
- 611 Somma, R., Iuliano, S., Matano, F., Molisso, F., Passaro, S., Sacchi, M., Troise, C. and De Natale, G.: High-resolution morpho-  
612 bathymetry of Pozzuoli Bay, southern Italy, *Journal of Maps*, 12, 2, 222-230,  
613 <https://doi.org/10.1080/17445647.2014.1001800>, 2016.
- 614 Tarquini, S., Isola, I., Favalli, M., Battistini, A. and Dotta, G.: TINITALY, a digital elevation model of Italy with a 10 meters  
615 cell size (Version 1.1), Istituto Nazionale di Geofisica e Vulcanologia (INGV), <https://doi.org/10.13127/tinitaly/1.1>, 2023.
- 616 Tinti, S., Bortolucci, E. and Vannini, C.: A block-based theoretical model suited to gravitational sliding, *Natural Hazards*, 16,  
617 1-28, <https://doi.org/10.1023/A:1007934804464>, 1997.
- 618 Tinti, S., Pagnoni, G. and Zaniboni, F.: The landslides and tsunamis of 30th December 2002 in Stromboli analysed through  
619 numerical simulations, *Bulletin of Volcanology*, 68, 462-479, doi: 10.1007/s00445-005-0022-9, 2006.
- 620 Triantafyllou, I., Zaniboni, F., Armigliato, A., Tinti, S. and Papadopoulos, G. A.: The Large Earthquake (~M7) and Its  
621 Associated Tsunami of 8 November 1905 in Mt. Athos, Northern Greece, *Pure Appl. Geophys.*, 177, 1267-1293,  
622 <https://doi.org/10.1007/s00024-019-02363-5>, 2020.



- 623 Vilibić, I., Šepić, J., Rabinovich, A. B. and Monserrat, S.: Modern approaches in meteotsunami research and early warning,  
624 *Frontiers in Marine Science*, 3, 57, <https://doi.org/10.3389/fmars.2016.00057>, 2016.
- 625 Zaniboni, F. and Armigliato, A.: Worst-case tsunami approach applied to Catania (eastern Sicily). In Sørensen, M., Behrens,  
626 J., Jalayer, F., Løvholt, F., Lorito, S., Rafliana, I., Salgado, M., Selva, J. (eds), *Probabilistic Tsunami Hazard and Risk Analysis*,  
627 Springer Nature, Switzerland, 2025 (in publication).
- 628 Zaniboni, F., Pagnoni, G., Paparo, M. A., Gauchery, T., Rovere, M., Argnani, A., Armigliato, A. and Tinti S.: Tsunamis From  
629 Submarine Collapses Along the Eastern Slope of the Gela Basin Strait of Sicily, *Front. Earth Sci.* 8, 602171, doi:  
630 [10.3389/feart.2020.602171](https://doi.org/10.3389/feart.2020.602171), 2021.
- 631 Zaniboni, F., Pagnoni, G., Gallotti, G., Tinti, S. and Armigliato, A.: Landslide-tsunamis along the flanks of Mount Epomeo,  
632 Ischia: propagation patterns and coastal hazard for the Campania Coasts, Italy. In Marotta, E., D'Auria, L., Zaniboni, F., Nave,  
633 R. (eds), *Volcanic Island: from Hazard Assessment to Risk Mitigation*, Geological Society, London, Special Publications, 519,  
634 <https://doi.org/10.1144/SP519-2020-128>, 2024.
- 635 Zollo, A., Maercklin, N., Vassallo, M., Dello Iacono, D., Virieux, J. and Gasparini, P.: Seismic reflections reveal a massive  
636 melt layer feeding Campi Flegrei caldera, *Geophysical Research Letters*, 35, 12, <https://doi.org/10.1029/2008GL034242>,  
637 2008.